Joint International Topical Meeting on Mathematics & Computation and Supercomputing in Nuclear Applications (M&C + SNA 2007)
Monterey, California, April 15-19, 2007, on CD-ROM, American Nuclear Society, LaGrange Park, IL (2007)

COMPUTER SIMULATION OF BUBBLE FORMATION

Insepov Z. *
Argonne National Laboratory
9700 South Cass Ave, Argonne 60439 IL
insepov@anl.gov

Bazhirov T., Norman G., Stegailov V.,
Institute for High Energy Densities of
Joint Institute for High Temperatures of RAS
Izhorskaya St. 13/19, Moscow 125412, Russia
bazhirov@ihed.ras.ru; norman@ihed.ras.ru; stegailov@ihed.ras.ru;

ABSTRACT

Properties of liquid metals (Li, Pb, Na) containing nanoscale cavities were studied by atomistic Molecular Dynamics (MD). Two atomistic models of cavity simulation were developed that cover a wide area in the phase diagram with negative pressure. In the first model, the thermodynamics of cavity formation, stability and the dynamics of cavity evolution in bulk liquid metals have been studied. Radial densities, pressures, surface tensions, and work functions of nano-scale cavities of various radii were calculated for liquid Li, Na, and Pb at various temperatures and densities, and at small negative pressures near the liquid-gas spinodal, and the work functions for cavity formation in liquid Li were calculated and compared with the available experimental data. The cavitation rate can further be obtained by using the classical nucleation theory (CNT). The second model is based on the stability study and on the kinetics of cavitation of the stretched liquid metals. A MD method was used to simulate cavitation in a metastable Pb and Li melts and determine the stability limits. States at temperatures below critical ($T < 0.5Tc$) and large negative pressures were considered. The kinetic boundary of liquid phase stability was shown to be different from the spinodal. The kinetics and dynamics of cavitation were studied. The pressure dependences of cavitation frequencies were obtained for several temperatures. The results of MD calculations were compared with estimates based on classical nucleation theory.

Key Words: Bubble, cavity, liquid metals, nucleation theory, simulation

1. INTRODUCTION

Computer simulations are capable of studying interactions of fission gases with nuclear fuels, structural materials and coolant, radiation damage and defect accumulation processes. Atomistic simulation methods, such as Molecular Dynamics (MD), is a powerful method for studying diffusion of fission gases and an initial stage of the cavitation process in liquid and solid metals that are of interest of fusion and fission programs.

Gas bubble formation can significantly contribute to nuclear fuel aging and fracture. It is also important for the fusion reactor first wall development at high D+, He+ fluxes from the plasma

* Corresponding author

when liquid metal becomes saturated with the light atoms [1]. Enhanced sputtering characteristics of low-energy light ions bombarding a liquid Li surface and the diffusion properties of such elements in liquid metal have attracted much attention because of the important feasibility studies of using liquids as a plasma-facing component (PFC) for future tokamak devices [2].

Liquid sodium is the coolant material for fast reactors and its void formation characteristics are important to mitigate the accidents when the void activation coefficient becomes positive. Liquid lead is a basic component of the promising heat-transfer materials in the new type of power reactors with fast deuterium-tritium fuel ignition [3]. The performance of such systems is substantially deteriorated by continuity loss (cavitation) in the heat-transfer material. This is caused by the negative stresses that arise due to microexplosions in the working chamber. Therefore, the cavitation kinetics in the heat transfer material under dynamic tensile stresses is an important task which should be solved, in order to control the system functioning.

MD study of the gas bubble and cavity formation in simple bulk liquids is a well studied area of statistical mechanics [4-18]. Classical nucleation theory (CNT) has been reviewed in [4]. Density profiles $\rho(r)$, normal and tangential components of the pressure tensor $P_N(r)$ and $P_T(r)$, using both the Irving-Kirkwood and Harashima definitions of P were obtained in [5] where these variables were applied to define the surface tension of a Lennard-Jones fluid. The surface tension of a LJ fluid was determined by MD simulation in [6-8] by using Tolman's length in the limit of small curvatures. The calculated Tolman's length was positive in [6-9]. MD study of water at elevated temperatures was conducted in [9]. By using a Nosé-Hoover thermostat and a truncated and shifted LJ interatomic potential, the authors of [10] concluded that there is no curvature dependence of the surface tension which contradicts to the results of other papers. The probability of finding a void in a LJ liquid was studied in [11].

Surface tension of bubbles and droplets followed to a Tolman's relation was found in [12, 13] where a LJ potential was employed. However, the surface tension of bubbles was obtained to be much less (15% of the planar surface) strongly deviating form that of a droplet which has much bigger difference compared to the flat surface.

Spinodal lines (or Thermodynamic Limit of Metastability - TLM) for monatomic and diatomic liquid oxygen modeled via one- and two-center LJ interatomic potentials were calculated by MD in [14]. A Kinetic Limit of Metastability (KLM) which defined as a lowest density at which the liquid was homogeneous, was also calculated

A nonequilibrium MD method was employed to study a local liquid heating that was generating bubbles in Ref. [16]. After an energy exchange of the bubbles with the ambient liquid, the bubbles are cooled down and eventually dissolved in the bulk liquid. The authors compared the microscopic dynamics of the bubble dissolution obtained by MD with the results of the hydrodynamic Rayleigh-Plesset equation; and they have confirmed that the hydrodynamics is reliable even at such small scales.

Structure of a curved interface and many physical properties of bubbles, droplets and cavities in a LJ-liquid were studied by a MC method in [17-19] and by analytical methods such as Density Functional (DF) method, generalized van der Waals, and a Mean-Field theory in [20-23].
The aim of this paper is to develop a method of studying metastable liquids at negative pressures, by calculating stability, normal and tangential pressure tensors, density and Gibbs energy of the stable nucleus, by using MD simulation method.

Studies of cavitation are of great interest for practical applications and theory because this phenomenon is frequently encountered in practice in processes accompanied by metastable liquid formation and because studies of cavitation allow the mechanisms of new phase formation to be understood more thoroughly. The traditional method for describing the kinetics of cavitation is classic nucleation theory based on thermodynamic calculations of the work of new phase nucleus formation and solution of the kinetic equation for the size distribution of nuclei [24-27]. The use of classic nucleation theory in practice, especially at negative pressures, is often complicated by uncertainty in the actual accuracy of model concepts on which the theory is based and the absence of both reliable data on surface tension at the inter phase boundary and the equation of state of metastable liquids. The use of classic nucleation theory is also limited as concerns closeness of the phase state to the phase stability limits (spinodal).

The MD method allows cavitation to be studied at a microscopic level, solely on the basis of the selected interatomic interaction potential, and without additional assumptions on the mechanisms of cavity formation and growth. For instance, cavitation in a Lennard-Jones liquid was studied by the MD method in [28, 29], where the influence of the cutoff radius of interparticle interaction potentials was analyzed. The appearance and growth of a localized vapor nucleus was clearly seen in a system of 10976 particles [30]. A method for calculating the frequency of homogeneous nucleation in a metastable phase simulated by the MD method was suggested in [30-33] for the example of nucleation in a superheated crystal. This method was based on averaging the metastable phase lifetime over an ensemble of independent MD trajectories.

The aim of this paper is to develop a computer simulation method that will enable bubble, cavity and void stability and growth when light ions/atoms are implanted into liquid Li, Pb, Na, and nuclear fuels by using MD and Computational Fluid Dynamics (CFD) methods.

In the present work, MD with a realistic interatomic potential for Pb was used to study the stability limits of liquid lead and the kinetics of cavitation at large negative pressures and temperatures substantially lower than critical ($T < 0.5\ Tc$). The results of MD simulations are compared with classic nucleation theory predictions.

2. COMPUTATIONAL MODELS AND METHOD

Structure and dynamical properties of liquid Li and lead were studied by MD at various temperatures and densities along the melting line for solid lithium and far below this line. A few different effective inter-ionic potential for liquid Li and Pb were used in this work [34-36]. The trajectories of atomic motions were calculated by the numerical integration of a system of classical equations of motion using the difference scheme of the second order of accuracy.

Constant temperatures were set and maintained using the Langevin thermostat scheme. An MD model of bubble nucleation is developed based on the classical nucleation theory. According to this theory, nucleation of the bubble is a process controlled by an energy barrier which is defined by interplay between the volume and surface energy contributions into the total system. This energy barrier defines the critical bubble radius: bubbles smaller than the critical one tend to shrink their sizes and collapse; those bubbles that are larger – tend to continuously grow.

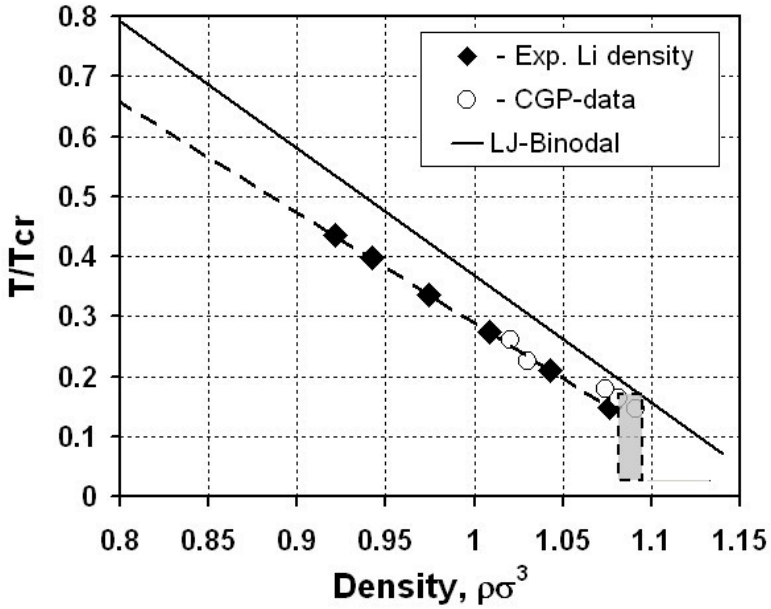

Fig. 1. Phase diagram for liquid Li. Dash line and diamonds – experimental liquid lithium densities [37], open circles – the parameters for five liquid Li potentials developed in [38]. The density is given in the reduced units $\rho\sigma^3$ ($\sigma = 2r_0$, $r_0 = 2.9051$Å); solid line is the LJ-binodal [39]. The shaded area shows the parameters of liquid lithium that were used to model cavities in this work.

2.1. Thermodynamics of Small Cavity

Structure and dynamical properties of liquid Li were studied by MD at various temperatures and densities along the melting line for solid lithium. Two different types of effective inter-ionic potential for liquid Li were used for this work. The first potential was developed for five different temperatures: 470, 525, 574, 725, and 843 ºK and corresponding densities, ρ, g/cm^3: 0.513, 0.508, 0.505, 0.484, and 0.480, along the melting line in [38] (CGP-potential).

The second Li-Li potential was developed based on a local density approximation and is given in an analytic form [40] (LBP-potential). This potential is convenient for modeling liquid Li surface by MD method as it is available for wide temperature and density ranges. For a system with N atoms, the total potential energy of the ionic sub-system can be represented as:

$$U_{\text{coh}} = U_{\text{el}} + U_{\text{rep}},$$

Where U_{el} is electronic energy and U_{rep} is the repulsive ionic interaction represented by the Born-Mayer potential:

$$U_{el} = -\sum_i \left\{ \sum_{j \neq i} \varsigma^2{}_0 \exp\left[-2q\left(\frac{r_{ij}}{r_0} - 1 \right) \right] \right\}^{1/2}$$
$$U_{rep} = \sum_i \varepsilon_0 \sum_{j \neq i} \exp\left[-p\left(\frac{r_{ij}}{r_0} - 1 \right) \right], \quad (1)$$

where ε_0, r_0 are the equilibrium energy depth and interionic distance, ς_0^2 is the hopping integral, and p, q are the dimensionless parameters that fit the potential and they are given in [40]. Interatomic interactions between lead particles were modeled via a glue many-body EAM potential for Pb developed in [41].

Although the liquid metal used as a plasma facing material of the fusion device in reality contain gases such as hydrogen or helium, two our MD bubble models consider cavities containing only metal atoms, i.e. without any light ions or atoms. Such simplification of the model is based on the calculation results that the total energies, pressure tensors, and surface tensions of the cavities do not drastically change if helium atoms were placed inside the cavity, due to a weak interaction of helium with lithium. Our models do not applicable to hydrogen bubbles as hydrogen can form a chemically stable hydride with metals. Therefore, this model can be a valid approximation of the helium bubbles in plasma facing fusion materials.

We obtained radial pressures around a bubble in liquid in analogy with the droplet capillary theory [5, 21]. Similar approach was used in [12, 13] where bubble formation and their stability were studied by MD in a LJ-system.

$$P(r) = P_N(r) + P_{Tr}(r),$$
$$P_T(r) = P_N(r) + \frac{r}{2}\frac{dP_N(r)}{dr},$$
$$P_N(r) = P_{Kin}(r) + P_U(r),$$
$$P_{Kin}(r) = \rho(r) k_B T,$$
$$P_U(r) = -\frac{1}{4\pi r}\sum_k \left| \vec{r} \cdot \vec{r}_{ij} \right| \frac{1}{r_{ij}} \frac{dU(r_{ij})}{dr_{ij}}, \quad (2)$$
$$\gamma_S^3 = -\frac{1}{8}(P_l - P_g)\int_0^\infty r^3 \frac{dP_N}{dr} dr.$$

The average radial densities $\rho(r)$ and pressures were calculated as a ratio by dividing the number ΔN of particles confined within a narrow spherical layer dr to the value of dr:

$$\langle \rho(r_k) \rangle = \left\langle \Delta N / \Delta r \right\rangle_k, k = 1 \cdots n, \quad (3)$$

$P_N(r)$ is the normal and $P_{Tr}(r)$ the transverse components of the the pressure tensor $P(r)$ of the cavity and r is the distance from the center of the cavity. See the details in ref. [5] where similar formulas were used for an exactly opposite case – droplet formation in gas. $P_{Kin}(r)$ is the kinetic and $P_U(r)$ - the potential terms of the pressure, U is the interaction potential for which an EAM many – body potential was used, P_l and P_g are the liquid and the gas pressures inside the cavity.

$$R_S = \frac{2\gamma_S}{P_l - P_g}, \qquad R_e = \frac{1}{\rho_l - \rho_g}\int_0^\infty r^3 \frac{d\rho}{dr} dr. \tag{4}$$

R_s is the the radius of the surface of tension and R_e – the equimolecular dividing radius [13].

$$\gamma_S \Big/ \gamma_\infty = 1 - \frac{2\delta}{R_S}, \ \delta = R_e - R_S \tag{5}$$

Where γ_S – the bubble surface tension, γ_∞ – the surface tension of a flat plane, δ – a typical thickness of the curved interface, and δ/R_s is a small parameter in the Tolman's formula (4).
The surface tension of the cavity gives the free energy barrier according to the main CNT formula:

$$\Delta\Omega(r) = -\frac{4}{3}\pi r^3 \cdot \Delta\omega + 4\pi r^2 \cdot \gamma_S, \qquad \Delta\omega = P_g - P_l \tag{6}$$

Where the first term is a volume gain contribution (a negative) term and the second term – is the surface energy loss contribution (a positive) term.

According to the CNT, nucleation of a microscopic bubble is a process controlled by the energy barrier which is defined by interplay between the volume and surface free energy contributions into the total energy. This energy barrier defines the critical bubble radius: bubbles smaller than the critical one tend to shrink in size and eventually collapse; those bubbles that are larger than the critical one – tend to continuously grow. Therefore, the MD models developed in this work should be able to predict the energy barrier (or work function) and the critical bubble size.

Two different MD models of bubble formation were developed in this paper. First model defines the critical radius of the bubble by using the CNT theory and using MD as a means for obtaining the surface tension of the cavities in liquid metal. As an example, this model was applied to cavities in liquid lithium.

According to the second model, the rate of a spontaneous phase transition was defined by a mean number of critical nuclei formed in unit volume per unit time, that is, by the cavitation frequency J. In this work, the cavitation frequency was calculated as $J = 1/(<\tau>V)$, $<\tau>$ is the mean lifetime, V is the simulation box volume.

In this work, we considered systems with up to 10^5 atoms in the simulation box. Three-dimensional periodic boundary conditions were used. The trajectories of atomic motions were calculated by the numerical integration of a system of classical equations of motion using the difference scheme of the second order of accuracy with a 1 fs time step. Constant temperatures were set and maintained using a Langevin thermostat scheme.

2.2. Kinetics of Cavitation

2.2.1. Computational model

Interatomic interactions are described by a many-particle potential for Pb, Li from the set of embedded atom model potentials [40, 41] suggested in [36]. Interaction energy can then be represented by the sum of two terms.

$$E = \sum_{i<j} \phi(r_{ij}) + \sum_i F(\bar{\rho}_i) \tag{7}$$

The first term corresponds to a pair interaction potential. The second term describes many-particle interactions, the embedding function F in it depends on the effective electron density on atoms. The latter is in turn a function of the distance between atoms,

$$\bar{\rho}_i = \sum_{j \neq i} \rho(r_{ij}) \tag{8}$$

The Pb potential parameters were adjusted in [36] using the condition of correspondence to the properties of the crystalline phase (its binding energy, surface energy, elastic constants, phonon frequencies, thermal expansion, and temperature of fusion). This potential was successfully used to study surface and cluster fusion and crystallization and vaporization of nanoclusters [42]. It was, for instance, shown that the temperatures of fusion (618 ± 4 K) and vaporization (~2050 K) of MD models based on this potential were in close agreement with the experimental values for lead (600.7 and 2033 K, respectively). In addition, because of the inclusion of the many-particle contribution, embedded atom potentials describe the behavior of particles on an open surface and therefore all phenomena related to liquid–gas phase transitions better than pair potentials.

In this work, we considered systems with from 13500 to 500000 atoms in the basic cube. Three dimensional periodic boundary conditions were used. The trajectories of atomic motions were calculated by the numerical integration of a system of classical equations of motion using the difference scheme of the second order of accuracy with a 1.43 fs time step. The instantaneous temperature (T*)* and pressure (p) averaged over the cell volume were calculated as

$$T = \frac{2m}{3k_B N} \sum_{i=1}^{N} \frac{\mathbf{v}_i^2}{2}, \qquad P = \frac{1}{V}\left(Nk_B T + \frac{1}{2} \sum_i \vec{F}_i \vec{r}_i \right), \tag{9}$$

where k B is the Boltzmann constant, m is the mass of the atom, V is the calculation cell volume, and $F\,i$ is the force acting on particle i . Constant temperatures were set and maintained using the thermal stabilization scheme (a thermostat), that is, additional Langevin terms were introduced into the equations of motion, namely, self-consistent white noise and friction [43], whose total influence was small compared with that of interatomic interaction forces.

The initial configuration of atoms corresponding to the liquid phase was generated as follows. First, a configuration which was a face centered cubic (FCC) lattice of atoms with the required density $\rho = mN / V$ and velocities randomly selected according to the Maxwell distribution corresponding to temperature T was constructed. Liquid metastable states at density and temperature values that excluded the possibility of solid phase existence were studied. For this reason, the lattice underwent fusion in several dozen femtoseconds during MD trajectory calculations, and the system became a liquid with the given temperature T, which was then maintained by the thermostat for several picoseconds. The final configuration of preliminary MD calculations was the sought initial configuration. We used different initial velocity distributions corresponding to the same temperature and density to produce an ensemble of independent initial configurations corresponding to the liquid at given ρ and T.

2.2.2. The stability limits of the metastable liquid phase

We considered cavitation in the liquid at large negative pressures corresponding to states close to the stability limits (spinodal). Experimental data on liquid metal spinodals (including Pb spinodal) are currently unavailable. General liquid phase spinodal characteristics in the region of negative pressures at low temperatures ($0 < T < 0.5\ T$ c) have also been studied poorly (e.g., see [44]). The position of the spinodal of liquid lead can be preliminarily estimated on the basis of MD calculations of the spinodal of a Lennard-Jones fluid [45] using the concept of thermodynamic similarity with respect to the critical parameters (Fig. 1a). We therefore performed preliminary estimates of negative pressures corresponding to a strongly stretched metastable lead melt in the temperature range studied.

Spinodal position calculations for the MD model under consideration were performed by calculating the p–ρ dependence along isotherms and determining the $(dp/d\rho)_T = 0$ point by extrapolation (see Fig. 1b). MD trajectories 100–200 ps long were calculated for all densities at a fixed temperature. The degree of metastability was low at high densities (for instance, at $\rho > 9.8$ g/cm^3 for $T = 1000$ K), and no cavitation occurred in the system during the time of computations.

The lifetime of metastable liquids τ decreases as the density lowers, and cavitation can occur during computations. Isotherms were constructed by averaging pressure p over the MD trajectory portion up to the beginning of the phase transition ($0 < t < \tau$). Because the selection of the extrapolation function is uncertain (we used polynomials of degrees $n = 2$–4), spinodal points are determined not unambiguously, to within ~7% for p and ~3% for $\rangle$. Figure 1b shows that stability loss in calculations at lower temperatures occurs earlier than $(dp / d\rho)_T$ becomes zero. The stability loss and $(dp / d\rho)_T = 0$ points approach each other as the temperature increases

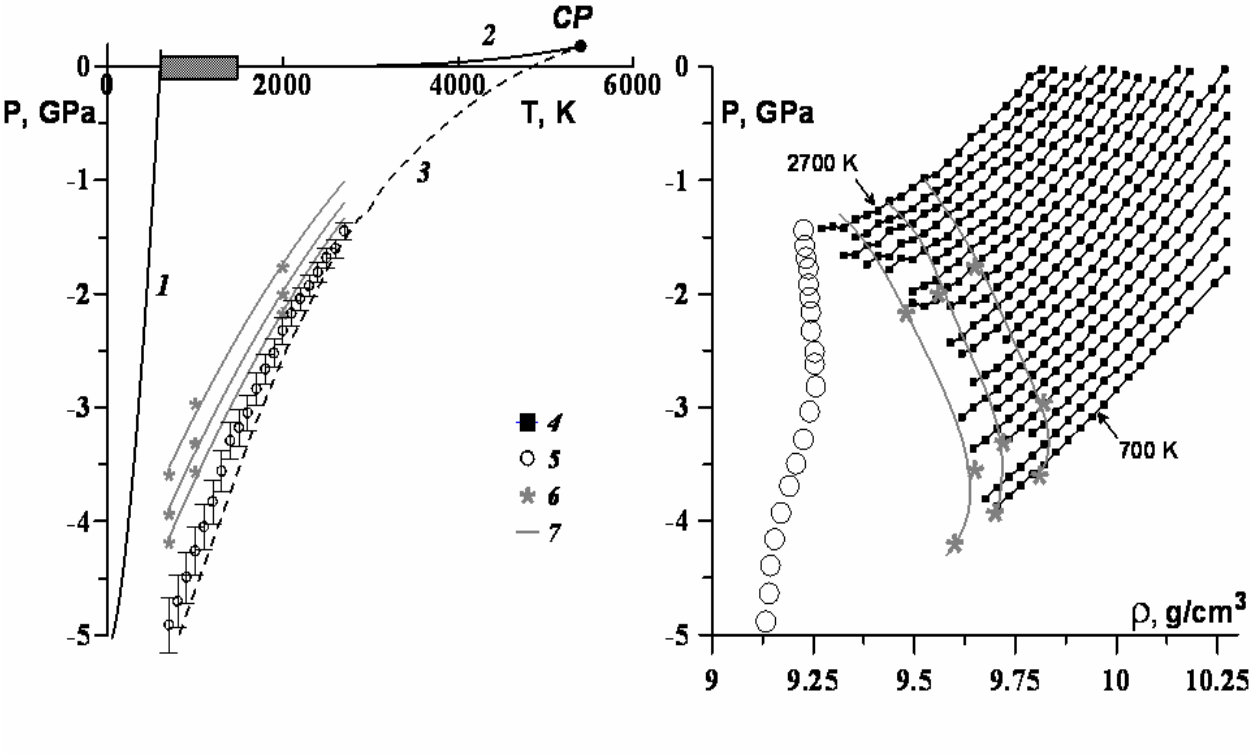

Fig. 2. *p*–*T*–ρ diagram of lead: (a) (*1*) experimental melting curve and its extrapolation to negative pressures by the Simon equation $p/p* = (T/Tm)c - 1$ ($p* = 5.11$ GPa, $Tm = 600$ K, and $c = 1.65$), (*2*) vaporization curve, and (*3*) liquid lead spinodal estimated by the renormalization of the Lennard-Jones system spinodal with the use of critical point parameters ($Tc = 5400$ K and $pc = 0.175$ GPa [47]); the hatched region corresponds to the supposed coolant working parameters in FIHIF reactors [48,49]; (b) isotherms of liquid lead over the temperature range 700–2700 K drawn in steps of 100 K; points *4* obtained in MD calculations are linked by solid lines for clearness (also see [50]). Common to (a) and (b): *5* labels the points at which $(dp/d\rho)_T = 0$ for the approximation of lead isotherms by polynomials (see Fig. 2b (1b), *6* corresponds to the points at 700, 1000, and 2000 K at which the cavitation rate is 10^{28}, 10^{29}, and $3 \cdot 10^{29}$ cm^{-3}/s (the closer the point to the spinodal the higher the corresponding cavitation rate), and points *7* are estimated points at which the cavitation rate has one of the values specified above over the temperature range 700–2700 K.

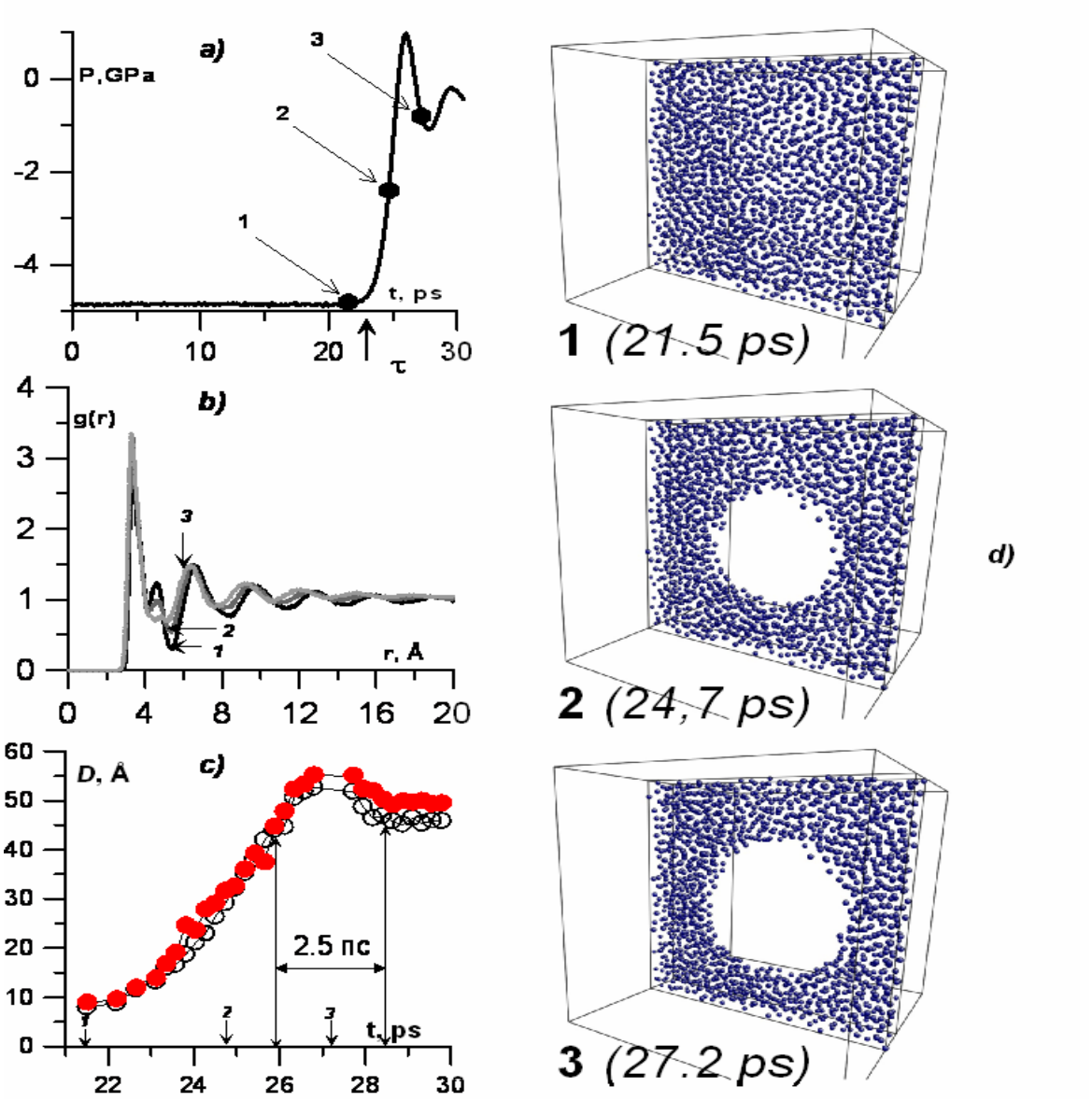

Fig. 3. (a) Instantaneous pressure *p* values depending on time *t* during spontaneous decomposition of the stretched liquid (300 K, τ is the metastable state lifetime along the given MD trajectory); numbers correspond to system configurations shown in Fig. 2d, configurations *1*, *2*, and *3* correspond to time moments 21.5, 24.7, and 27.2 ps, respectively; (b) pair correlation functions for time moments *1*, *2*, and *3* (see Fig. 2a); (c) dependence of the cavity diameter on time along axes *x* and *y* at 300 K and the degree of stretching with respect to the density at zero pressure equal to 1.19; the characteristic time of one oscillation (its half-period) is also shown; and (d) sections of the calculation cell atomic structure corresponding to states *1*, *2*, and *3* in Fig. 2a; section *1* contains a metastable liquid phase before cavity formation, section *2* corresponds to the beginning of cavity formation, and section *3* shows the cavity formed.

The calculated values are somewhat larger than those obtained in preliminary spinodal estimates by similarity relations (comparison should take into account possible errors in the experimental lead critical parameters). The closeness of the calculation results and preliminary spinodal estimates may be evidence of universal similarity of the spinodals of simple liquids at low temperatures. We stress that the interatomic interaction models actually compared, that is, the Lennard- Jones pair potential with an interaction radius of up to three coordination spheres and the many-particle embedded atom potential with an interaction radius of up to two coordination spheres, are qualitatively different. Note in addition that, as distinct from the results for a Lennard-Jones system [45, 46], the Pb melt spinodal does not intersect the continuation of the line of lead melting into the region of negative pressures according to the Simon equation, which is evidence that the crystal and liquid can be at equilibrium over the whole range of metastable states.

2.2.3. Cavity formation

The time dependence of pressure in the calculation cell along one MD trajectory is shown in Fig. 3a. Numbers *1 – 3* label system states before, during, and after cavity formation, respectively. The horizontal dependence portion corresponds to the liquid phase, and its length determines lifetime τ . The pair correlation functions $g(r)$ for system states from Fig. 3a are shown in Fig. 3b. We see that the shape of $g(r)$ changes during cavity formation. In particular, the second poorly defined peak disappears. The calculation cell sections corresponding to the system configurations specified in Fig. 3a are shown in Fig. 3d. Visual examination (with taking into account the symmetry parameter of atoms also) did not reveal crystal traces in the cell. Cavitation in the model under consideration is in character random homogeneous nucleation because of the absence of surface effects and spatial inhomogeneities in the periodic boundary conditions. The instant when cavity formation begins depends on local fluctuations of particle velocities and distances between the particles that form a nucleus of the new phase (cavity). According to visual estimates, the critical nucleus size corresponds to the volume of no more than 10–100 atoms in the density and temperature regions studied. For this reason, periodic boundary conditions do not influence the initial cavitation stage. Explosive cavity growth results in rapid stretched liquid unloading. When the cavity becomes commensurate in size with the calculation cell, the influence of periodic boundary conditions becomes substantial and requires a separate study (continuous medium equations [29] can be used to describe cavity growth into the region of supercritical sizes). The cavity ceases to grow with time in our model, and its size oscillates for some time (two or three complete oscillations) before it takes on a stationary value. Oscillations then die down. The characteristic time of oscillations (their half-period) is ~2.5–3 ps (see Fig. 3c).

We observed the appearance and growth of several nuclei simultaneously at 1000 and 2000 K. The lifetime of the system (up to a pressure jump) was then determined by the appearance of the first nucleus. The number of nuclei in the calculation cell and the rate of their appearance were largely determined by the proximity to the spinodal. The number of cavities formed during the time of computations increased as the size of the system grew (Fig. 5).

2.2.4. Cavitation rate

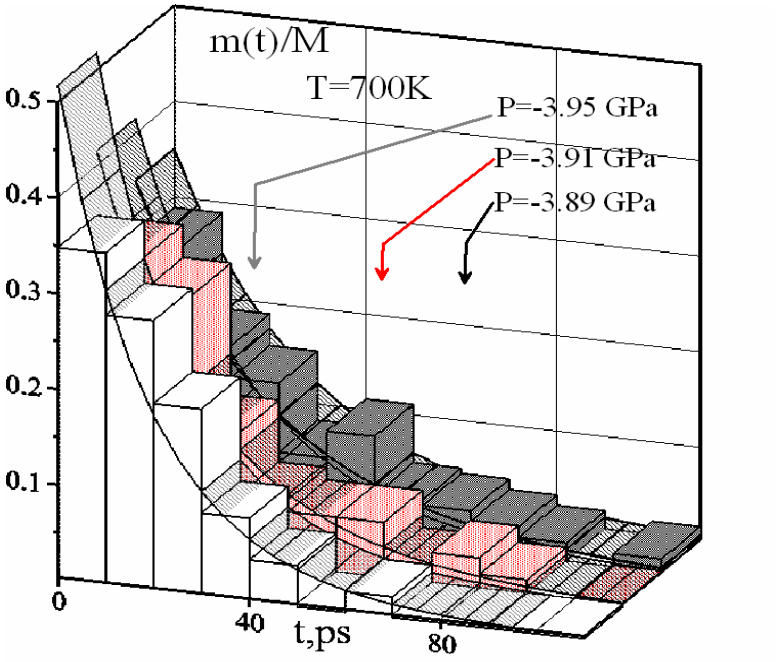

Fig. 4. Number of MD trajectories $m(\tau)$ from the ensemble of M independent trajectories. For each of the $m(\tau)$ trajectories, the instant of the beginning of cavitation (lifetime τ_i) lies in the interval $(\tau, \tau + \Delta\tau)$. Calculation results for various pressure p values at $T = 700$ K are shown ($\Delta\tau = 15$ ps): (*1*) $p = -3.95$ GPa, $M = 46$; (*2*) $p = -3.91$ GPa, $M = 232$; and (*3*) $p = -3.89$ GPa, $M = 142$. For comparison, the dependences obtained for the model according to which cavitation is a random Poisson process (2) are shown by straight lines (planes).

The lifetime of a uniform metastable liquid phase along one MD trajectory depends on the initial configuration and distribution of particle velocities and, the initial conditions being equal, integration step [29,32]. Statistical averaging for the given thermodynamic state (ρ, T, p) is performed over an ensemble of M independent initial configurations, each characterized by the corresponding lifetime τ_i ($i = 1, \ldots, M$). According to the model that treats homogeneous nucleation as a random Poisson process, the distribution of lifetimes τ_i over the ensemble of initial configurations has the form [24, 25]

$$m(\tau) = \frac{M \cdot \Delta\tau}{\bar{\tau}} \exp\left(-\frac{\tau}{\bar{\tau}}\right), \qquad \bar{\tau} = \frac{1}{M}\sum_{i=1}^{M} \tau_i \tag{10}$$

where $m(\tau)$ is the number of trajectories from the ensemble of M trajectories along which cavitation occurs during the $(\tau, \tau + \Delta\tau)$ time interval and is the mean lifetime. Examples of distributions obtained in our calculations are shown in Fig. 4.

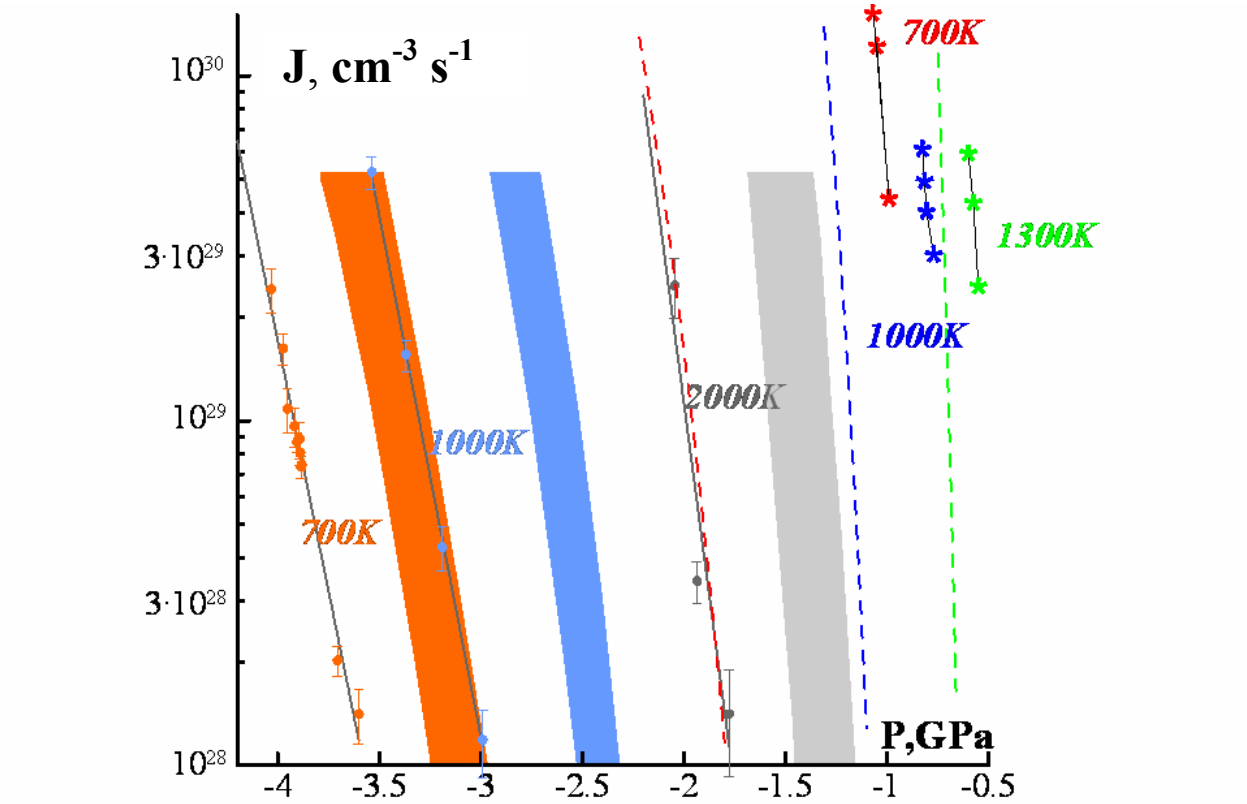

Fig. 5. Pressure *p* dependences of cavitation rate *J* along three isotherms: 700 (orange), 1000 (baby blue), and 2000 K (gray) for Pb and 700 (red), 1000 (blue) and 1300 K (green) for Li. Calculation results (solid circles for Pb and stars for Li) are given with errors corresponding to the error in mean lifetime determination. The filled areas and dashed lines of the *J*–*p* plane regions correspond to calculations according to (3) for the temperatures specified above taking into account errors in surface tension values σ for liquid lead (for liquid lithium this error was not considered).

We see that model (2) fairly well describes the cavitation process under consideration. The obtainment of distributions with a well-defined exponential form requires the accumulation of a large statistic ($M > 100–200$). The root-mean square error in determined from M measurements is $\sigma_{\bar{\tau}} = \bar{\tau}/\sqrt{M}$ for the exponential distribution law. The rate of a spontaneous phase transition is usually characterized by the mean number of critical nuclei formed in unit volume per unit time, that is, by the cavitation rate J. In this work, the cavitation rate was calculated as $J = 1/(\bar{\tau}\ V)$. The calculation results are shown in Fig. 5.

4. RESULTS AND DISCUSSION

Helium bubble nucleation and growth in liquid Li was simulated by MD method and compared with the classical nucleation theory. The classical nucleation theory of bubble formation in liquids predicts the existence of a critical bubble radius [39]. According to this theory, bubbles smaller than a critical bubble size should eventually be dissolved in liquid. Those bubbles that are larger than the critical one should grow. Upon continuous growing, such bubbles move toward the open surface and eventually blow up, thus producing splashing and macroscopic erosion of the liquid surface.

The lifetime of a uniform metastable liquid phase along one MD trajectory depends on the initial configuration and distribution of particle velocities and, the initial conditions being equal, integration step. Statistical averaging for the given thermodynamic state (ρ, T, p) is performed over an ensemble of M independent initial configurations, each characterized by the corresponding lifetime τ_i (i = 1, M). Homogeneous nucleation can be described as a random Poisson process. We see this model fairly well describes the cavitation process under consideration. The obtainment of distributions with a well-defined exponential form requires the accumulation of a large statistic (M > 100–200). Generating of a big number of trajectories for statistical analysis is a very efficient task for the parallel calculations on a computer clusters. The rate of a spontaneous phase transition is usually characterized by the mean number of critical nuclei formed in unit volume per unit time, that is, by the cavitation frequency J. In this work, the cavitation frequency was calculated as $J = 1/(<\tau>V)$, $<\tau>$ is the mean lifetime, V is the simulation box volume. The calculation results qualitatively correctly reproduce classic nucleation theory estimates, but quantitative agreement worsens as the temperature increases. This difference can be interpreted as systematic lowering of the work W of critical nucleus formation in the approach [4]. The discrepancy between theory and calculation results can be decreased by including the dependence of surface tension on surface curvature. The existing models of the nuclear fuel bubbles due to fission gases release were analyzed and feasible models were discussed. A Computational Fluid Dynamics model of large bubbles in nuclear fuels was developed and the results were compared to the atomistic simulation results.

4.1. Energy barrier for cavity formation in liquid Li

Fig. 6 (a-f) shows six cavities that were placed in the middle of the computational cell in liquid Li at a liquid density of 0.480 g/cm^3. The temperatures of the system were scaled down a stable cavity was obtained and were below the binodal line shown in Fig. 1 by a dash-line. Each cavity was equilibrated until the temperature was not stabilized within ~ 10 ps, and after that the physical properties such as the radial density, pressure tensors, and surface tensions were calculated. If the temperature showed growth by more than 5% of the initial one, the initial temperature was decreased and the simulation started again, until a stable cavity was obtained.

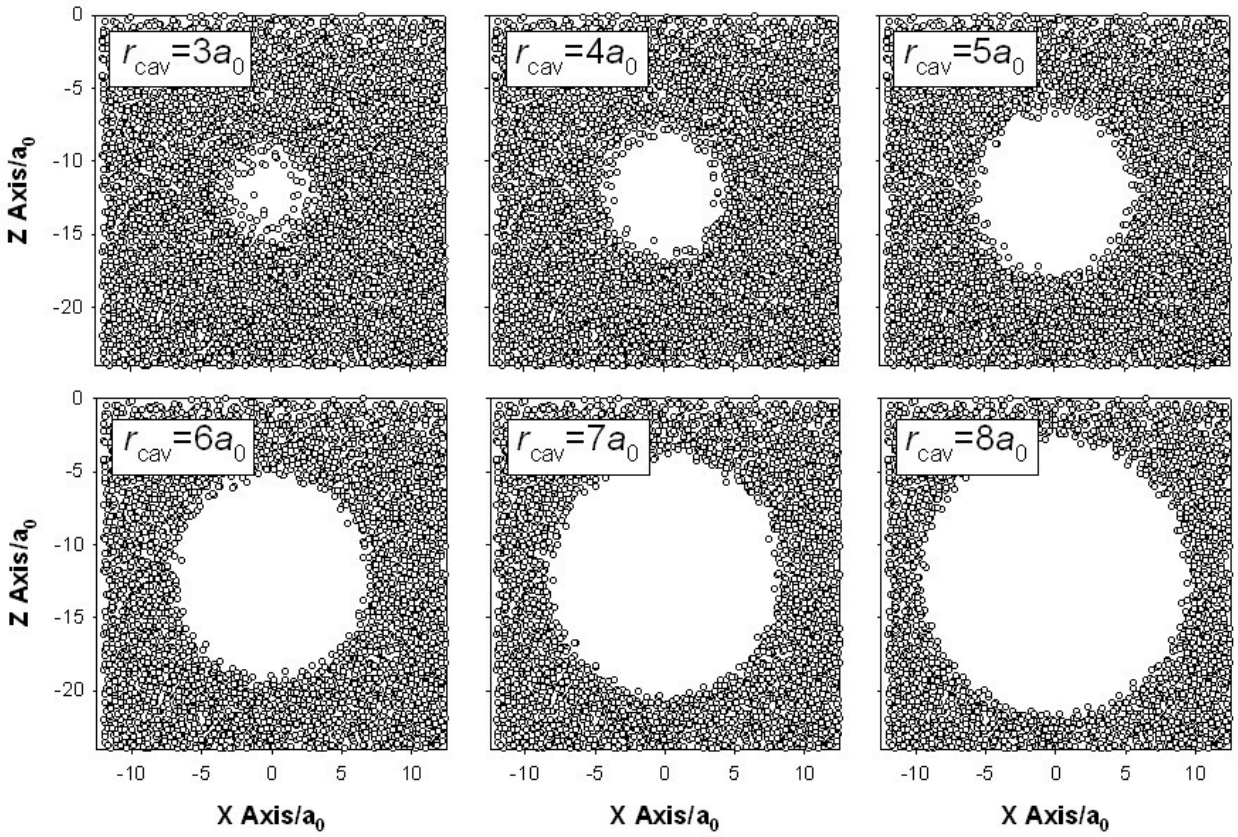

Fig. 6a-f). Cavities studied in this work with the following radii: a) 3, b) 4, c) 5, d) 6, e) 7, and f) 8a_0, where a_0 is the Li bcc lattice parameter obtained from the density as: $a_0 = (2m_0/\rho)^{1/3}\times10^8$ Å; m_0=1.15257×10^{-23} g, is the Li atomic mass.

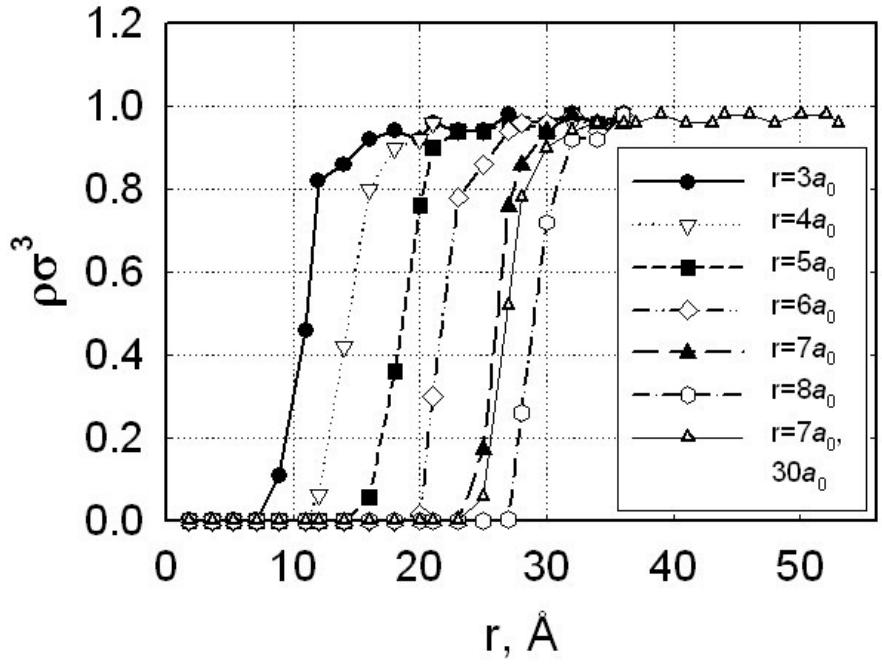

Fig. 7. Radial density for six stable cavity sizes at 100°K in reduced units where $\sigma = 2r_0$. (r_0 = 2.9052 Å)

The next figure 8 (4) shows the normal component of the pressure tensor for all cavities modeled in this work.

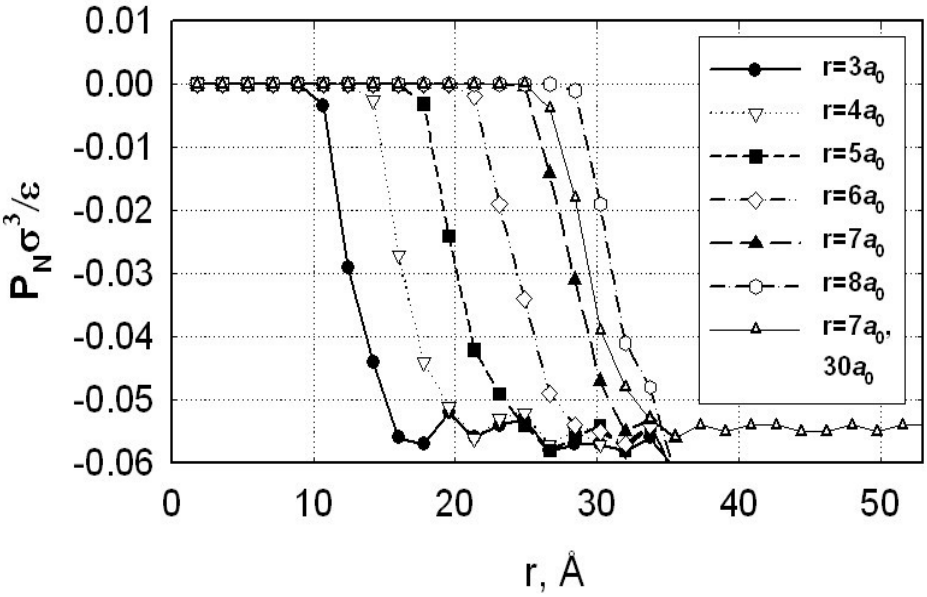

Fig. 8. Radial component of the pressure tensor at 100ºK in reduced units where $\sigma = 2r_0$ (r_0 = 2.9052 Å and ε = 1 eV).

By using formulas (2-5), the surface tensions were calculated for all cavity sizes and all temperatures (Fig. 9 (5). Fitting of the calculated results for the surface tension to the Tolman's formula is shown in Fig. 10a (6a). This comparison shows a drastic difference between the surface tension ratio for the plane surface; and these results are a few times are higher than the Tolman's data. Fig. 10b (6b) shows our main calculated results for the free energy barrier obtained in this work for the first time. One cavity with the radius $7a_0$ was calculated twice with the different system sizes of $20a_0$ and $30a_0$. It clearly shows that there exists an energetic barrier in compliance with the CNT of new phase formation.

4.2. Cavitation rate in liquid Pb

The calculation results are interesting to compare with classic nucleation theory predictions. Let us use the temperature dependence of the rate of nucleation determined according to Zel'dovich (see [4, 24]) as:

$$J = \frac{\rho}{m}\sqrt{\frac{2\sigma}{\pi m}}\exp\left(-\frac{W}{k_B T}\right), \quad W = \frac{16\pi\sigma^3}{3(P-P')^2} \qquad (11\ (3)$$

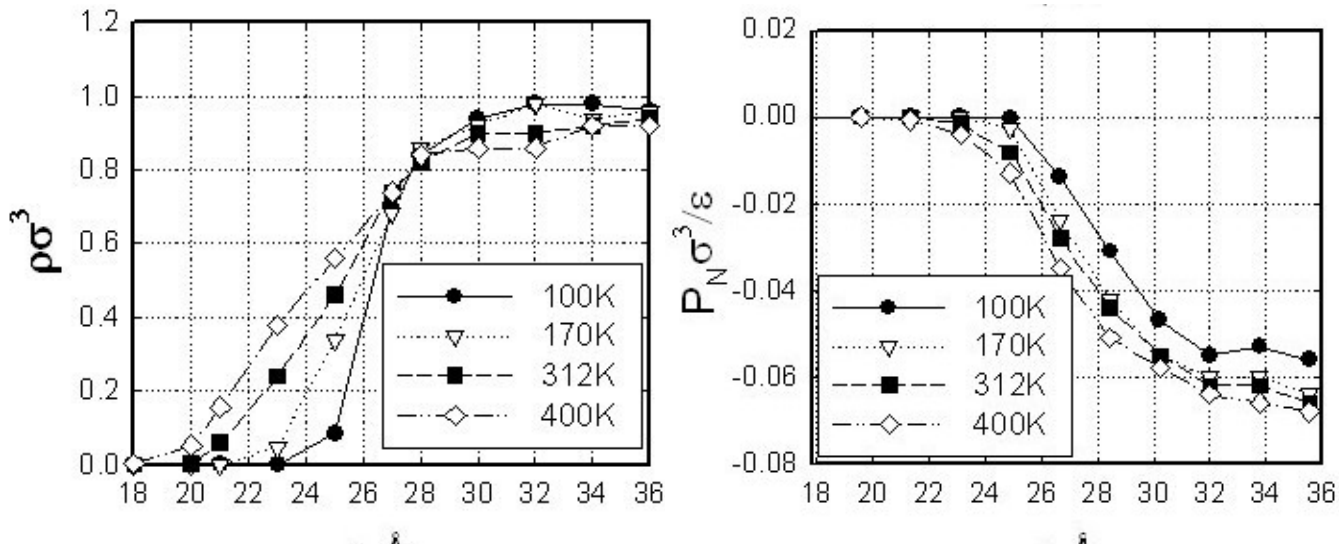

Fig. 9. Temperature dependence of the radial density and the radial component of the pressure tensor for the cavity with the radius of $7a_0$, in reduced units where $\sigma = 2r_0$ (r_0 and ε are the same as in Fig. 7,8).

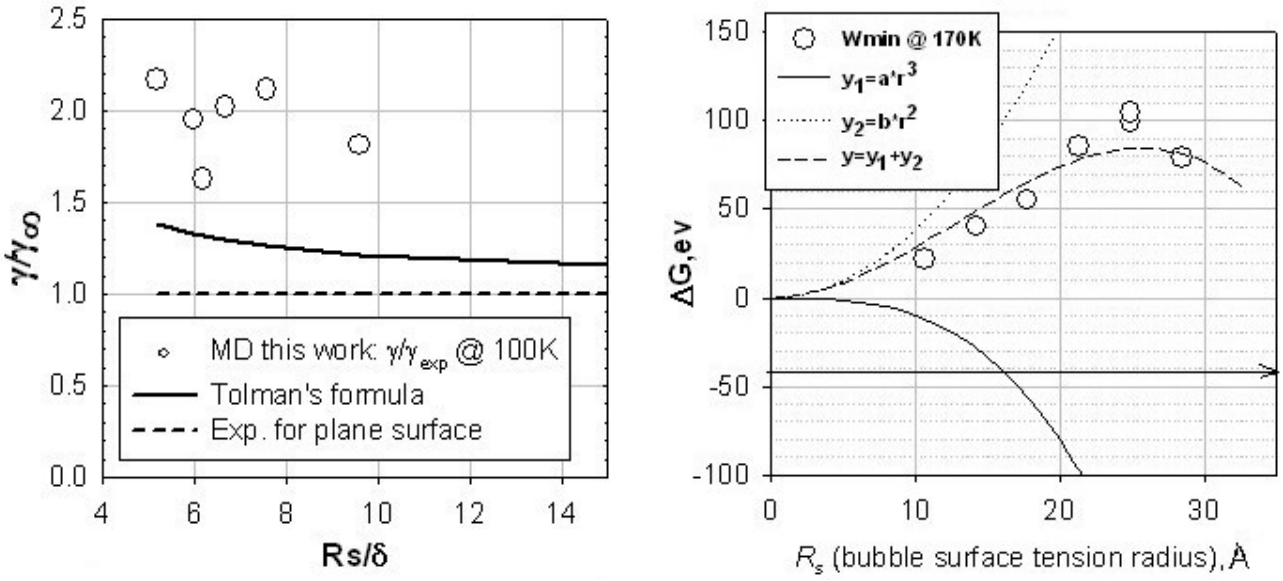

Fig. 10. a) Fitting the results for surface tension obtained by these MD calculations to the Tolman's formula (see eq. 5). b) Free energy barrier calculated by formula 6 in this work for six cavities. One cavity with the radius $7a_0$ was calculated twice with the different system sizes of $20a_0$ and $30a_0$.

where σ is the surface tension along the vaporization line at temperature T, W is the work of critical nucleus formation, and p' is the vapor pressure in the critical nucleus. Approximation 11 was selected because of the simplicity of the pre-exponential factor, which only contained σ of all the special metastable liquid parameters. Equation 11 was compared with the results of MD calculations on the assumption that the pressure in the system containing a critical nucleus was equal to the mean pressure along the metastable region ($0 < t < \tau$) and the vapor pressure in the critical bubble was negligibly low, $p' << p$. The latter assumption was used because the density of vapor at low temperatures ($T < 0.5T$c) was low and critical bubbles were virtually empty. Bubble growth corresponded to the transfer of holes (vacancies) from the liquid rather than the transfer of molecules into the vapor phase. We used the experimental data on the surface tension of molten lead along the vaporization line [50]. The surface tension σ very strongly influences the work of critical nucleus formation and, therefore, the temperature and pressure dependences of the nucleation rate. For this reason, the spread of experimental data was included in the form of the confidence interval $\sigma_{min} < \sigma < \sigma_{max}$ heuristically constructed on the basis of the uncertainty of the linear approximation of experimental data in the region of high temperatures [51]. Equation (3) was therefore used to obtain the $J(p, \sigma)$, $\sigma_{min} < \sigma < \sigma_{max}$, regions.

It follows from Fig. 5 that the calculation results qualitatively correctly reproduce classic nucleation theory estimates, but without quantitative agreement. When (11) is used, this difference can be interpreted as systematic lowering of the work W of critical nucleus formation. The discrepancy between theory and calculation results can probably be decreased by including the dependence of surface tension on surface curvature (e.g., see [24, 52]). The calculation results may be evidence that the surface tension of bubbles of the critical size is larger by 5–10% than its value for a plane interface. Note that a consistent comparison of MD simulation results and various classic nucleation theory approximations should involve the independent determination of the temperature dependence of surface tension along the liquid–vapor equilibrium line performed using the same MD model. Although the calculation results are in acceptable agreement with the classic nucleation theory approximation under consideration, the critical nucleus size estimated by this theory is $N_n = (\rho/m)\,(4\pi/3)\,(2\sigma/|P|)^3 \approx 1$ atom (ρ/m = 2.82×10^{28} м$^{-3}$, T = 700K, σ = 0.431 N/m, P = -3.89 GPa), which is, generally, outside the applicability range of the macroscopic classic nucleation theory approach in the region under consideration.

Our consideration of cavitation is limited to homogeneous nucleation in pure lead. The homogeneous nucleation frequency is exponentially small far from the stability limits of the metastable liquid because of the high activation barrier to spontaneous fluctuation cavity formation. Cavitation in a coolant in the practically important region of power plant functioning parameters should largely occur by the heterogeneous mechanism of nucleation on impurities and inhomogeneities (such as, for instance, lithium atoms in the Li17Pb83 eutectic [48, 49]). MD heterogeneous cavitation rate calculations can be performed using a correct model of interactions with impurity atoms. Homogeneous cavitation in molten lithium was considered in [53].

Since the selected method of calculations can be used at various numbers of particles, the question arises of the extent to which the results depend on the size of the calculation cell. We determined the particle number dependencies of metastable liquid pressure and temperature at realistic particle number values (from 500 to 500000 particles in the cell). It was found that the

size of the system substantially influenced parameter fluctuations with respect to their mean values rather than the mean values themselves, in accordance with theoretical predictions. As concerns the influence of the system size on the rate of cavitation, the cavitation rate was independent of volume because the number of critical nuclei increased as the volume grew (Fig. 11.

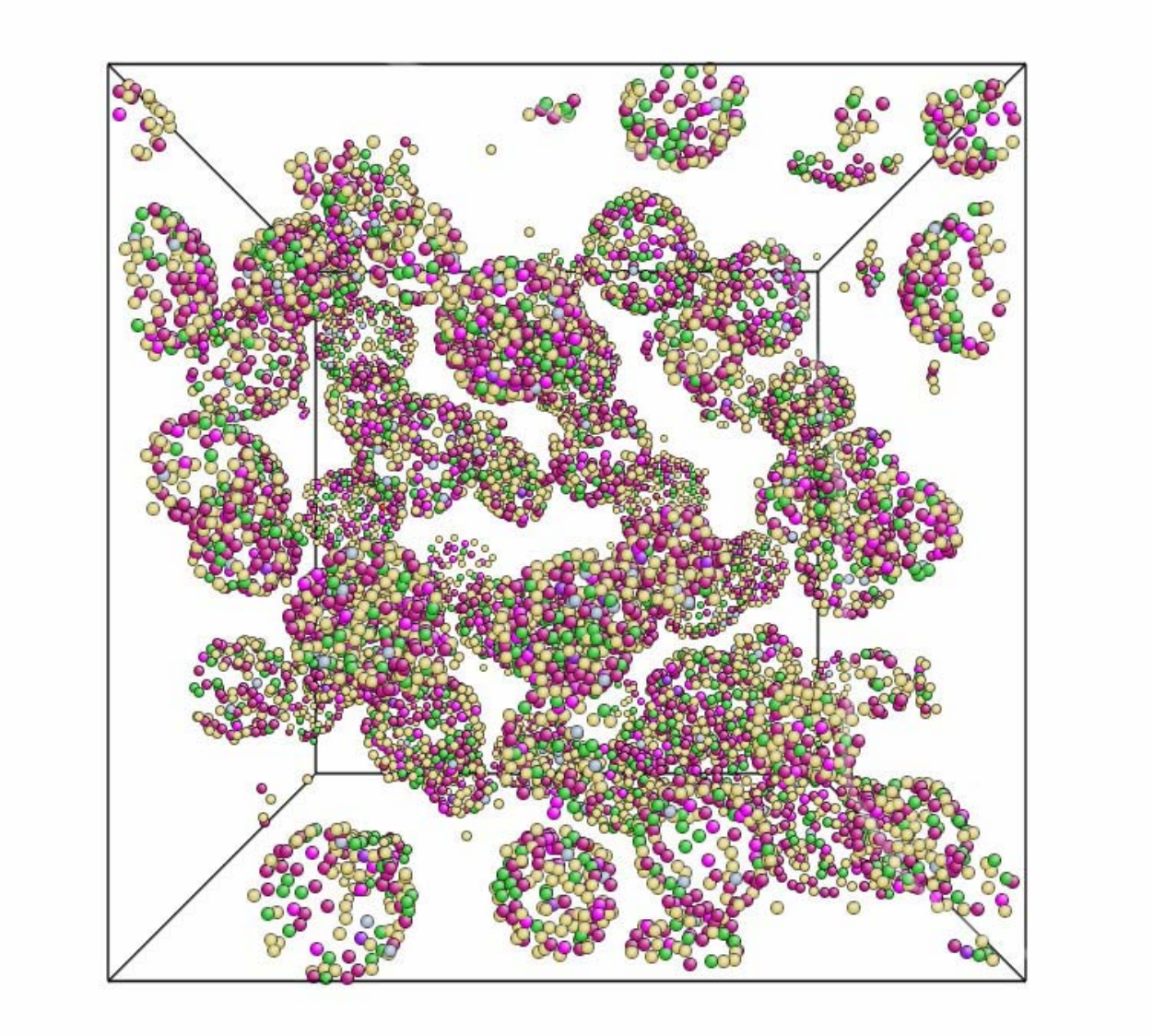

Fig. 11. Image of the calculation cell (500000 atoms) with only the atoms largely situated at cavity boundaries and having the smallest number of neighbors in a sphere of a certain radius selected from clearness considerations.

On the other hand, the degrees of metastability obtained experimentally cannot be studied by the MD method because of a comparatively long metastable phase lifetime. On the whole, the ratio between the volume of the calculation cell and the lifetime is only determined by system closeness to the spinodal. Clearly, when we infinitely increase the volume of a system, it can be treated as a collection of small volumes (the number of particles in such a small volume should

at least be sufficient for the formation of a new phase nucleus), where cavitation occurs independently. As was shown, the probability of the appearance of a nucleus in each small volume had a Poisson distribution. It is then clear that the larger the system, the higher the probability of formation of the first cavity in a shorter time in it. In our view, the number of nuclei in a unit substance volume is volume-independent. The same reasoning explains the formation of a large number of cavities as the size of the system increases. The preliminary results were published in [51].

4. CONCLUSIONS

The rate (frequency) of cavitation (nucleation) is $J = 1/(\bar{\tau}\ V)$. The question arises of how the results of our calculations can be extrapolated to the region of large volumes. Indeed, at $J =$ const, we find that the metastable phase lifetime vanishes in macroscopic volumes (V–>∞). Currently, MD simulations are performed for small volumes, whose lifetime can be determined in numerical experiments. Clearly, the state of a substance as close to the spinodal as in numerical experiments can hardly be obtained experimentally. For this reason, macroscopic substance volumes cannot exist at the degrees of proximity to the spinodal attainable in MD experiments.

Bubble formation and growth in liquid Li was also studied by simulating the nucleation and growth of cavities of various sizes in a bulk liquid Li system by MD method. Our results show that the small cavities will be easily dissolved in a liquid at 470K. However, if the cavity size becomes larger than a critical one, the cavity grows. We conclude that bubble formation mechanism in liquid Li has a high probability in saturated states.

A MD method with the realistic interatomic potential for Pb was deployed to calculate the homogeneous cavitation rate pressure dependence in liquid lead under negative pressure near the liquid spinodal. The results of MD simulations are not in agreement with the simple classic nucleation theory approach. At the moment it is not clear if this discrepancy can be attributed to the shortcomings of the potential or the kinetic model deployed. However the method presented gives the possibility of the direct calculation of the cavitation rate. Currently the similar calculations are carrying out for liquid Li and Pb-Li alloy under negative pressures.

Bubble formation in liquid metals (Li, Pb) was studied by MD simulation method by employing many-body EAM-potentials the nucleation and growth of cavities of various sizes in a bulk liquid Li system by MD method. Six cavity sizes with the radii of r_{cav} = 10-30Å were modeled at the density of 0.480 g/cm³ and at various temperatures below the binodal curve on the phase diagram of the liquid lithium.

The radial densities, normal and tangential pressure tensors, surface tensions and free energy barrier of small cavities in liquid lithium were calculated at various temperatures.
This MD simulation has confirmed the existence of the critical radius of the cavity in liquid metal for the first time. We also showed that the cavity formation in liquid Li complies well with the predictions of the classical nucleation theory. However, the surface tensions obtained by MD simulations are more than 2 times higher than those predicted by classical nucleation theory for a flat surface.

We conclude that bubble formation mechanism in liquid Li has a high probability in saturated states. It could significantly contribute to surface erosion thus explain recent controversial experimental results.
The MD method with the realistic interatomic potential for Pb was deployed to calculate the homogeneous cavitation rate pressure dependence in liquid lead under negative pressure near the liquid spinodal. The results of MD simulations are not in agreement with the simple classic nucleation theory approach. At the moment it is not clear if this discrepancy can be attributed to the shortcomings of the potential or the kinetic model deployed. However the method presented gives the possibility of the direct calculation of the cavitation rate. Currently the similar calculations are carrying out for liquid Li and Pb-Li alloy under negative pressures.

SOFTWARE USED AND CALCULATION FEATURES.

To provide an ability of fast parallel calculations we have used LAMMPS free MD simulation package: http://lammps.sandia.gov. It has built-in MPI support. MD problems are easy to compute parallel because of particular procedure of particle numeration and interatomic force calculation. In addiction the method of cavitation rate calculation mentioned above is also easy make parallel: the need to have a variety of independent initial configuration and hence of independent MD trajectories let us compute each MD trajectory on a single processor (or single cluster also possible).

ACKNOWLEDGMENTS

This work was partially supported by U.S. Department of Energy, under Contract DE-AC02-06CH11357, and by the Russian Ministry of Education and Science (project RNP.2.1. 1.712) and the RFBR grant 05-08-65423.

REFERENCES

1. A. Hassanein, “Liquid metal targets for high-power applications: pulsed heating and shock hydrodynamics”, *Laser and particle beams*, **18**, pp. 611-622 (2000).
2. L. B. Begrambekov, A. M. Zakharov, A. A. Pustobaev, V. G. Tel’kovskii, Transl. from Atomnaya Energiya, **64** (1988) 212-215.
3. S. Medin, M. Basko, M. Churazov, et al., “Power plant conceptual design for fast ignition heavy-ion fusion”, *Nucl. Instrum. Methods Phys. Res. A*, **544**, pp. 300-309 (2005).
4. M. Blander, J.L. Katz, “Bubble nucleation in liquids”, *AICHE J.*, **21**, pp. 833-848 (1975).
5. S.M. Thompson, K.E. Gubbins, J.P.R.B. Walton, R.A.R. Chuntry, J.S. Rowlinson, “A Molecular Dynamics study of liquid drops”, *J. Chem. Phys.* **81** (1984) 530-542.
6. M.J.P. Nijmeijer, A.F. Bakker, C. Bruin, J.H. Sikkenk, “A Molecular Dynamics simulation of the Lennard-Jones liquid-vapor interface”, *J. Chem. Phys.* **89** (1988) 3789-3792.
7. M.J.P. Nijmeijer, C. Bruin, A.B. van Woerkom, A.F. Bakker, “Molecular Dynamics of the surface tension of a drop”, *J. Chem. Phys.* **96** (1992) 565-576.
8. M.J. Haye, C. Bruin, “Molecular Dynamics study of the curvature correction to the surface tension”, *J. Chem. Phys.* **100** (1994) 556-559.

9. R.D. Mountain, “Voids and clusters in expanded water”, *J. Chem. Phys.* **110** (1999) 2109-2115.
10. H. El Bardouni, M. Mareshal, R. Lovett, M. Baus, “Computer simulation study of the local pressure in a spherical liquid-vapor interface”, *J. Chem. Phys.* **113** (2000) 9804-9809.
11. D.M. Huang, D. Chandler, “Cavity formation and the drying transition in the Lennard-Jones fluid”, *Phys. Rev.* E **61** (2000) 1501-1506.
12. S.H. Park, J.G. Weng, C.L. Tien, “Cavitation and bubble nucleation using molecular dynamics simulation”, *Microscale Thermophysical Engineering*, **4** (2000) 161-175.
13. S.H. Park, J.G. Weng, C.L. Tien, “A molecular dynamics study on surface tension of microbubbles”, *Intern. J. Heat & Mass Transf.*, **44** (2001) 1849-1856.
14. T. Tokumasu, K. Kamijo, M. Oike, Y. Matsumoto, “Molecular dynamics study of the nucleation of bubble”, In: *CAV 2001*: 4th Intern. Symp. Cavit., 2001, California Institute of Technology, Pasadena, CA USA.
15. C. Xiao, D.M. Heyes, “Cavitation in stretched liquids”, *Proc. R. Soc. Lond.* A **458** (2002) 889-910.
16. H. Okumura, N. Ito, “Nonequilibrium molecular dynamics simulation of a bubble”, *Phys. Rev.* E **67** (2003) 045301 (R).
17. J.K. Lee, J. Barker, G.M. Pound, “Surface structure and surface tension: pertubation theory and Monte Carlo calculation”, *J. Chem. Phys.* **60** (1974) 1976-1980.
18. V.K. Shen, P.G. Debenedetti, “A computational study of homogeneous liquid-vapor nucleation in the Lennard-Jones fluid”, *J. Chem. Phys.* **111** (1999) 3581-3589.
19. M.P. Moody, P. Attard, “Curvature dependent surface tension from a simulation of a cavity in a Lennard-Jones liquid close to coexistence”, *J. Chem. Phys.* **115** (2001) 8967-8977.
20. O. Sinanoglu, “Microscopic surface tension down to molecular dimensions and microthermodynamic surface areas of molecules or clusters”, *J. Chem. Phys.* **75** (1981) 463-468.
21. D.J. Lee, M.M. Telo da Gama, K.E. Gubbins, “A microscopic theory for spherical interfaces: liquid drops in the canonical ensemble”, *J. Chem. Phys.* **85** (1986) 490-499.
22. M.A. Hooper, S. Nordholm, “Generalized van der Waals analysis of critical drops and cavities in simple fluids”, *J. Chem. Phys.* **87** (1987) 675-686.
23. R. McGraw, A. Laaksonen, “Interfacial curvature free energy, the Kelvin relation, and vapor-liquid nucleation rate”, *J. Chem. Phys.* **106** (1997) 5284-5287.
24. V. P. Skripov, *Metastable Liquid* (Nauka, Moscow, 1972) [in Russian].
25. V. P. Skripov and M. Z. Faizullin, *Crystal–Liquid–Vapor Phase Transitions and Thermodynamic Similarity* (Fizmatlit, Moscow, 2003) [in Russian].
26. V. P. Skripov and V. P. Koverda, *Spontaneous Crystallization of Supercooled Liquids* (Nauka, Moscow, 1984) [in Russian].
27. I.I. Novikov, *Thermodynamics of Spinodals and Phase Transitions* (Nauka, Moscow, 2000) [in Russian].
28. V. G. Baidakov and S. P. Protsenko, Dokl. Akad. Nauk **41**, 231 (2003).
29. V. G. Baidakov and S. P. Protsenko, Dokl. Akad. Nauk **394**, 752 (2004) [Dokl. Phys. **49** (2), 69 (2004)].
30. T. Kinjo and M. Matsumoto, Fluid Phase Equilib. **144**, 343 (1998).
31. G. E. Norman and V. V. Stegailov, Dokl. Akad. Nauk **386**, 328 (2002) [Dokl. Phys. **47** (9), 667 (2002)].
32. G. E. Norman and V. V. Stegailov, Mol. Simul. **30**, 397 (2004).

33. A. Yu. Kuksin, G. E. Norman, and V. V. Stegailov, in *Computational Physics: Proceedings of the Joint Conference of ICCP6 and CCP2003*, Ed. by X.-G. Zhao, S. Jiang, and X-J. Yu (Rinton Press, 2005), pp. 126–129.
34. M. Canales, J. A. Padro, L. E. Gonzalez, A. Giro, "Molecular dynamics simulation of liquid lithium" J. Phys. Condens. Matter **5** (1993) 3095-3102.
35. Y. Li, E. Blaisten-Barojas, D.A. Papaconstantopoulos, "Structure and dynamics of alkali-metal clusters and fission of highly charged clusters" *Phys. Rev.* B **57** (1998) 15519.
36. H.S. Lim, C.K. Ong, F. Ercolessi, "Stability of face-centered cubic and icosahedral lead clusters", *Surface Science*, **269/270** (1992) 1109-1115.
37. R. W. Ohse (Ed.), *Handbook of Thermodynamic and Transport Properties of Alkali Metals*, Blackwell Scientific Publ., Oxford, 1985, p. 987.
38. M. Canales, L. E. Gonzalez, J. A. Padro, "Computer simulation study of liquid lithium at 470 and 843 K", *Phys. Rev.* E **50** (1994) 3656-3669.
39. F. Abraham, Homogeneous Nucleation, Academic Press, New York, 1974
40. D. K. Belashchenko, *Usp. Fiz. Nauk* **169**, 361 (1999).
41. D. K. Belashchenko, *Computer Modeling of Liquid and Amorphous Substances* (MISIS, Moscow, 2005) [in Russian].
42. G. Bilalbegovic and H. O. Lutz, *Chem. Phys. Lett.* **280**, 59 (1997).
43. A. A. Valuev, G. E. Norman, and V. Yu. Podlipchuk, in *Mathematical Modeling: Physico-Chemical Properties of Substances*, Ed. by A. A. Samarskii and N. N. Kalitkin (Nauka, Moscow, 1989), p. 5 [in Russian].
44. I. L. Iosilevskii and A. Yu. Chigvintsev, *Electronic Journal* "Made in Russia," http://zhurnal.ape.relarn.ru/artisles/ 2003/003.pdf (2003).
45. V. G. Baidakov and S. P. Protsenko, *Dokl. Akad. Nauk* **402**, 754 (2005) [Dokl. Phys. **50** (6), 303 (2005)].
46. V. G. Baidakov and S. P. Protsenko, *Phys. Rev. Lett.* **95**, 015701 (2005).
47. V. Ya. Ternovoi, V. E. Fortov, S. V. Kvitov, and D. N. Nikolaev, in *Shock Compression of Condensed Matter–1995*, Ed. by S. C. Schmidt and W. C. Tao (AIP, New York, 1996), Part 1, pp. 81–84.
48. S. A. Medin, Yu. N. Orlov, A. N. Parshikov, and V. M. Suslin, Preprint No. 41, IPM im. M. V. Keldysh RAN (Keldysh Institute of Applied Mathematics, Russ. Acad. Sci., Moscow, 2004).
49. S. Medin, M. Basko, M. Churazov, et al., Nucl. Instrum. Methods Phys. Res. **544**, 300 (2005).
50. *Physical Values: A Handbook*, Ed. by I. S. Grigor'ev and E. Z. Meilikhov (Energatomizdat, Moscow, 1991) [in Russian].
51. T. T. Bazhirov, G. E. Norman, and V. V. Stegailov, *Dokl. Akad. Nauk* **405** (3), 325–331 (2005) [*Dokl. Phys.* **50** (11), 570 (2005)].
52. J. W. P. Schmelzer, I. Gutzow, and J. Schmelzer, Jr, *J. Colloid Interface Sci.* **178**, 657 (1996).
53. Z. Insepov and A. Hassanein, *J. Nucl. Mater.* **337–339**, 912 (2005).